Atmos. Chem. Phys. Discuss., 13, 33013–33054, 2013
www.atmos-chem-phys-discuss.net/13/33013/2013/
doi:10.5194/acpd-13-33013-2013

Atmospheric Chemistry and Physics Discussions

Modeling of HCHO and CHOCHO at a semi-rural site in southern China during the PRIDE-PRD2006 campaign

X. Li[1,2], F. Rohrer[1], T. Brauers[1], A. Hofzumahaus[1], K. Lu[1,*], M. Shao[2], Y. H. Zhang[2], and A. Wahner[1]

[1]Institut für Energie- und Klimaforschung Troposphäre (IEK-8), Forschungszentrum Jülich, Jülich, Germany
[2]College of Environmental Sciences and Engineering, Peking University, Beijing, China
[*]now at: College of Environmental Sciences and Engineering, Peking University, Beijing, China

Received: 4 December 2013 – Accepted: 5 December 2013 – Published: 17 December 2013

Correspondence to: X. Li (x.li@fz-juelich.de) and A. Wahner (a.wahner@fz-juelich.de)

Published by Copernicus Publications on behalf of the European Geosciences Union.

Abstract

HCHO and CHOCHO are important trace gases in the atmosphere, serving as tracers of VOCs oxidations. In the past decade, high concentrations of HCHO and CHOCHO have been observed for the Pearl River Delta (PRD) region in southern China. In this study, we performed box model simulations of HCHO and CHOCHO at a semi-rural site in PRD, focusing on understanding their sources and sinks and factors influencing the CHOCHO to HCHO ratio (R_{GF}). The model was constrained by the simultaneous measurements of trace gases and radicals. Isoprene oxidation by OH radicals is the major pathway forming HCHO, followed by degradations of alkenes, aromatics, and alkanes. The production of CHOCHO is dominated by isoprene and aromatic degradation; contributions from other NMHCs are of minor importance. The modeled R_{GF} shows a complex dependence on the VOCs composition, OH and NO_x levels, and atmospheric physical processes, which suggest the necessity of careful treatment of R_{GF} as an indicator of anthropogenic or biogenic emissions. Compared to the measurement results, the model predicts significant higher HCHO and CHOCHO concentrations. Sensitivity studies suggest that this discrepancy is to a large extent (> 70 %) due to the missing consideration of fresh emissions, vertical transport of precursor VOCs, and uptake of HCHO and CHOCHO by aerosols in the model. Insufficient treatments of dry deposition of HCHO and CHOCHO and of vertical dilution of all species in the model account for the rest 30 % discrepancy. Our study indicates that, in addition to chemical mechanisms, atmospheric physical processes (e.g., transport, dilution, deposition) have to be well considered for a box model predicting HCHO and CHOCHO concentrations.

1 Introduction

The degradation of directly emitted volatile organic compounds (VOCs) results in the formation of ozone (O_3) and secondary organic aerosols (SOA) in the troposphere

ACPD
13, 33013–33054, 2013

(Finlayson-Pitts and Pitts, 2000). This process consists of the oxidation of VOCs by hydroxyl radical (OH), O_3, and nitrate radical (NO_3). Detailed understanding of the VOCs degradation mechanism is challenged by the co-existence of vast variety of VOCs species in the atmosphere. However, investigations on ubiquitous oxidation intermediates, e.g., formaldehyde (HCHO) and glyoxal (CHOCHO), can help us to test and improve the current knowledge of the VOCs sources and degradation pathways.

HCHO is the most abundant carbonyl compound in the atmosphere. Maximum HCHO concentrations can reach 100 ppb in polluted areas whereas sub-ppb levels are found in remote areas (Finlayson-Pitts and Pitts, 2000). Most of HCHO is produced during the oxidation of organic compounds (Fortems-Cheiney et al., 2012). While methane (CH_4) oxidation by OH radicals is the major source of HCHO in remote areas, the HCHO production in regions (e.g., forest, urban area) with elevated non-methane hydrocarbons (NMHCs) (i.e., alkanes, alkenes, aromatics, isoprene, and terpenes) is dominated by their degradation. Direct emissions of HCHO originate mainly from fossil fuel combustion (Schauer et al., 1999, 2002), biomass burning (Lee et al., 1997), and vegetation (DiGangi et al., 2011), but are usually of minor importance (Parrish et al., 2012). The known removal pathways of HCHO in the atmosphere are reaction with OH, photolysis, and dry/wet deposition. Heterogeneous uptake by cloud droplets and aerosols is speculated to be an additional sink of HCHO, which could contribute to the HCHO destruction (Zhou et al., 1996; Tie et al., 2001; Fried et al., 2003a). However, the existence of this process in the lower troposphere is still under discussion. Laboratory experiments indicate reactive loss of HCHO can happen on surfaces of H_2SO_4 aerosols (Jayne et al., 1996), mineral dust aerosols (Sassine et al., 2010), and organic aerosols (Li et al., 2011). Filed observations by Wang et al. (2010) suggest an uptake of HCHO by aerosols in the presence of amines (or ammonia) and carbonyl compounds. But, during a chamber study, Kroll et al. (2005) did not find any growth of both neutral ($(NH_4)_2SO_4$) and acidic (NH_4HSO_4) aerosols in the presence of gaseous HCHO, suggesting the uptake of HCHO by aerosols is unlikely taking place. Although numerical simulations of HCHO, either by multi-dimensional models or box models, can in

ACPD
13, 33013–33054, 2013

some cases reproduce HCHO observations (Wagner et al., 2001; Fried et al., 2003b; MacDonald et al., 2012), significant discrepancies between modeled and measured HCHO concentration have been frequently found (Choi et al., 2010; Fried et al., 2011, and references therein). The model underestimation can arise from: deviation from the steady-state assumption (Fried et al., 2003a), direct emissions and their transport (Fried et al., 2011), missing consideration of HCHO production from unmeasured precursors (Kormann et al., 2003; Choi et al., 2010), etc. If the steady-state assumption is disturbed, e.g., in the vicinity of fresh emissions, the model can also overpredict the measured HCHO concentration (Fried et al., 2011).

CHOCHO is the smallest dicarbonyl compound in the atmosphere. Ambient concentration of CHOCHO ranges from tens of ppt in remote and rural areas to ≈ 1 ppb in heavy polluted urban regions (e.g., Volkamer et al., 2007; Washenfelder et al., 2011; DiGangi et al., 2012). Compared to HCHO, CHOCHO has nearly no primary sources except biomass burning and biofuel combustion. Globally, isoprene and ethyne are the major precursors of CHOCHO (Fu et al., 2008). While local CHOCHO production is dominated by aromatics degradation in urban or sub-urban areas (Volkamer et al., 2007; Washenfelder et al., 2011), significant contributions from 2-methyl-3-buten-2-ol (MBO) and isoprene oxidation are identified for rural areas (Huisman et al., 2011). Removal of gaseous CHOCHO is driven by reaction with OH, photolysis, deposition, and loss on aerosol surfaces (Fu et al., 2008). By comparing CHOCHO column densities derived from a global model simulation to satellite observations, Myriokefalitakis et al. (2008) and Stavrakou et al. (2009) speculate of a missing global source of CHOCHO. Similar study performed recently by Liu et al. (2012) suggests that the missing CHOCHO sources in China is most likely due to the underestimation of aromatics in the VOCs emission inventory. As first indicated by Volkamer et al. (2007), if loss of CHOCHO on aerosol surfaces is not taken into account, models can substantially overestimate measured CHOCHO concentrations. Laboratory studies found that uptake of CHOCHO by aerosols is mainly through polymerization process and is related with the acidity and the ionic strength within the aqueous phase of aerosols (Jang and Kamens,

ACPD
13, 33013–33054, 2013

2001; Liggio et al., 2005; Kroll et al., 2005). Once CHOCHO is taken up by aerosols, it can contribute to the formation of secondary organic aerosols (Volkamer et al., 2007; Tan et al., 2009; Washenfelder et al., 2011).

Given that HCHO and CHOCHO have similar sinks but different sources, the CHOCHO to HCHO ratio (R_{GF}) has been proposed to be a tracer of changes of VOCs mixture in the atmosphere. Based on satellite observations, Vrekoussis et al. (2010) conclude that regions with R_{GF} lower than 0.045 are under influence of anthropogenic emissions, whereas R_{GF} higher than 0.045 often indicates that VOCs emissions mostly originate from biogenic sources. Average R_{GF} up to 0.2–0.4 were observed by MacDonald et al. (2012) in an Asian tropic forest. However, after analyzing the measured R_{GF} and relevant trace gases at a rural site, DiGangi et al. (2012) found that higher R_{GF} corresponded to increased anthropogenic impact on local photochemistry.

The Pearl River Delta (PRD) region located in southern China has been identified by satellite observations as the region with high levels of HCHO and CHOCHO (Wittrock et al., 2006; Vrekoussis et al., 2010). Yet simultaneous ground-based measurements of HCHO and CHOCHO in this region are quite limited. During the PRIDE-PRD2006 campaign, which was dedicated to the understanding of the formation mechanism of O_3 and SOA in this heavy polluted region, we performed one month of continuous MAX-DOAS observations for HCHO and CHOCHO at a semi-rural site in PRD (Li et al., 2013). The measured HCHO and CHOCHO concentrations as well as R_{GF} were as high as those obtained in other urban environments. Simultaneous measurements of HO_x ($= OH + HO_2$) radicals, trace gases, and aerosols suggest highly active photochemistry under the influence of both anthropogenic and biogenic emissions (Lou et al., 2010; Hu et al., 2012; Lu et al., 2012). In this paper, we will focus on investigating the production and destruction pathways of HCHO and CHOCHO during the PRIDE-PRD2006 campaign, and try to understand the change of R_{GF} with the change of airmass compositions.

ACPD
13, 33013–33054, 2013

2 Approach

2.1 Field measurements

The PRIDE-PRD2006 field campaign took place in July 2006 in the Pearl River Delta (PRD) region in southern China within the framework of the "Program of Regional Integrated Experiments of Air Quality over the Pearl River Delta" (PRIDE-PRD2006). Field measurements of HO_x radicals, trace gases, aerosols, and meteorological parameters were performed at a semi-rural site Back Garden (BG, 23.50° N, 113.03° E), which is located at the edge of PRD. While tens of kilometers south of the BG site big cities (i.e., Zhaoqing, Foshan, Guangzhou, and Dongguan) are located, north of it small towns prevail close to mountain areas which are typically covered by evergreen broad-leaf forest. The BG site is next to a water reservoir and is surrounded by farmland (peanuts, lychees, trees, small forests).

Concentrations of HCHO and CHOCHO were retrieved from MAX-DOAS scattered sunlight measurements at 6 elevation angles, using the method described in Li et al. (2013). During the retrieval, HCHO and CHOCHO are assumed to be well-mixed in a layer with height H. Using the retrieved vertical column densities (VCDs) and H, mean mixing ratios of HCHO and CHOCHO in the well-mixed layer were calculated. In order to exclude the influence of clouds on the MAX-DOAS retrieval, we only consider observations during cloud-free days. The systematic error of the retrieved HCHO and CHOCHO mixing ratios is around 35 %.

The MAX-DOAS measurements were performed in parallel with ground-based in-situ measurements of CO, CH_4, C3–C12 NMHCs, NO_x (= NO + NO_2), O_3, aerosol physical and chemical properties, photolysis frequencies, relative humidity, and pressure on top of a hotel building (10 m a.g.l.). Simultaneously, measurements of HO_x radicals, HONO, temperature, and 3-D-wind were performed on top of two stacked sea containers around 20 m away from the hotel building. Details of these measurements were described in separate papers (Lu et al., 2012, and references therein). Instrumentation, time resolution, and accuracy for parameters used in this study are listed in Table S1.

ACPD
13, 33013–33054, 2013

2.2 Model description

Concentrations of HCHO and CHOCHO were calculated by a zero-dimensional box model using the Master Chemical Mechanism Version 3.2 (http://mcm.leeds.ac.uk/MCM/). The model includes the full MCM chemistry for all measured NMHCs and their oxidation products. The model calculations were constrained to measurements of OH, NO, NO_2, HONO, O_3, CO, CH_4, C3–C12 NMHCs, photolysis frequencies, relative humidity, temperature, and pressure. Concentrations of ethane, ethene, and ethyne were fixed to 1.5 ppb, 3 ppb, and 1.7 ppb, respectively, estimated from few canister samples. H_2 mixing ratio was assumed to be 550 ppb. An additional loss process with a lifetime (τ_D) of 24 h was assumed for all calculated species. This lifetime corresponds to a dry deposition velocity of 1.2 cm s^{-1} and a well-mixed boundary layer height of about 1 km. The model was operated in a time-dependent mode for the entire campaign period (5–25 July), with 30 min time resolution and 2 days spin-up time. For periods when measured NMHCs data are not available, values were taken from the campaign mean diurnal variation. With regard to the missing OH values, they are estimated from the measured photolysis frequency of O_3 (J_{O1D}) using the empirical formula described by Lu et al. (2012). The model run with the above settings represents the current understanding on the HCHO and CHOCHO chemistry at the BG site, based on available precursor measurements. This base-case is called M0 in the text and figures. In order to investigate to which extent the model can reproduce the HCHO and CHOCHO measurements, different model scenarios were setup by including additional mechanisms in M0. Table 1 gives an overview of the employed model scenarios. In this study, we only focus on those 6 days when both HCHO, CHOCHO, NMHCs, and OH measurements were available, i.e., 12–13, 20–21, and 24–25 July.

2.3 Model uncertainty

The uncertainty of the model simulation of HCHO and CHOCHO can arise from the uncertainty of: (1) measured trance gas concentrations, (2) measured meteorological

ACPD
13, 33013–33054, 2013

parameters, i.e., photolysis frequencies J, temperature T, and pressure P, (3) reaction rate constants k used in the model, and (4) the lifetime τ_D for dry deposition. Using the same uncertainty factors listed in Table S7 in Lu et al. (2012), we run the model M0 for n times (n equals to the number of parameters been considered). During each model run, the value of the considered parameter is multiplied by its uncertainty factor. The model uncertainty is estimated by error propagation from the errors of all considered parameters. Gaussian error propagation was applied within each of the first three groups. The total model errors were then calculated conservatively by linear addition of the errors from all four groups. The mean diurnal variation of the uncertainty of the modeled HCHO and CHOCHO by the model base-case (M0) is shown in Fig. S1. On average, modeled HCHO and CHOCHO concentrations in the model base-case had an uncertainty of around 55 %.

3 Results

3.1 Measurements overview

The entire PRIDE-PRD campaign was characterized by tropical conditions with high temperature (28–36 °C), high humidity (60–95 % RH), and high solar radiation (indicated by noontime J_{NO_2} of (5–10) $\times 10^{-3}$ s^{-1}) (Li et al., 2012). These meteorological conditions, together with the prevailing emissions of air pollutants, are in favor of the high photochemical reactivity in the PRD region, which can be reflected by the measured high OH concentrations (noontime value of 1.5×10^7 cm^{-3}) and HO_x turnover rate (3×10^8 cm^{-3} s^{-1} around noon) (Hofzumahaus et al., 2009). For the 6 cloud-free days in this study, Fig. 1 shows the time series of measured wind speed, wind direction, OH reactivities of C2–C12 NMHC (k_{OH}^{NMHC}), OH concentrations, aerosol (PM_{10}) surface concentrations, aerosol (PM_1) compositions, and HCHO and CHOCHO concentrations. The wind speeds were generally below 3 $m s^{-1}$. According to the wind direction, air masses arriving at the BG site were mainly from two directions, i.e., south

ACPD
13, 33013–33054, 2013

on 20 and 21 July, north on 13, 24, and 25 July. On 12 July, the wind was from north in the first night, and became south during daytime, and changed back to north after sunset. Peak values of k_{OH}^{NMHC} were around 20 s^{-1} and normally occurred at night. Compared to southern wind days, elevated k_{OH}^{NMHC} with average values of 5.6–6.7 s^{-1} were observed in the period of 09:00–18:00 LT (local time, LT = UTC + 8 h) in northern wind days, which was mainly attributed to the higher isoprene concentrations. This is consistent with the fact that north of BG site is close to forest areas and air masses from north are therefore influenced by biogenic emissions. However, average OH reactivities of anthropogenic NMHC for the same period were nearly the same in the 6 days, e.g., $k_{OH}^{Alkene} \approx 1.2\,s^{-1}$, regardless of the origin of air masses. OH concentrations also does not show big difference in the 6 days, with peak values of 1.5×10^7 cm^{-3} around noon and values of 0–1 $\times 10^6$ cm^{-3} during night. The aerosol (PM_1) composition measurements found that almost half of the sub-micron aerosol mass was organics, followed by sulfate. On 24 and 25 July when strong combustion events happened in the surrounding areas, the aerosol mass and surface concentrations were significantly higher than in other days. The occurrence of the combustion events can be indicated by the increase of Cl^- concentration in PM_1 (Hu et al., 2012). This Cl^- increase is identified in the early morning of 13, 24, and 25 July and around mid-night of 25 July. Increase of k_{OH}^{Alkene} was also observed in the combustion periods. Given the change of NMHC composition and concentrations and the existence of primary emissions affecting the production of HCHO and CHOCHO, we separate the 6 measurement days into two groups in the following analysis. Group 1 (G1) includes 12, 20, and 21 July when air masses were mainly from south of the BG site. Group 2 (G2) represents 13, 24, and 25 July when air masses were from north of the BG site and were partly influenced by direct emissions from combustions. In the 6 cloud-free days, the measured average concentrations of HCHO and CHOCHO were 7.3 ppb and 0.37 ppb, respectively. Elevated HCHO and CHOCHO concentrations were observed during morning hours of G2 days, especially on 24 and 25 July. Diurnal variability of HCHO and CHOCHO was not very prominent. After excluding the periods influenced by direct emissions, a slight in-

ACPD
13, 33013–33054, 2013

crease of HCHO concentrations can be found from early morning to 12:00 LT, whereas CHOCHO concentrations are almost stable at around 0.3 ppb.

3.2 HCHO and CHOCHO simulation

The simulated HCHO and CHOCHO concentrations from the model base-case (M0) are shown in Fig. 2c and d. Neither the diurnal variation nor the concentration can be well reproduced by the model. The model predicts HCHO maxima occurring at around 09:00 LT with concentrations of 30–40 ppb. A decrease of HCHO concentration to 10–25 ppb is then predicted from late morning to afternoon. In the afternoon, the simulated HCHO are clearly separated into two groups; while the calculated concentrations are quite compact in each group, they are much higher in northern wind days (G2 days) than in southern wind days (G1 days). This phenomenon also exists for the modeled CHOCHO. However, the grouping of the simulation results becomes different in early morning hours. For HCHO, we see higher modeled concentrations on 12 and 25 July than on the other days. For CHOCHO, the elevated values are found on 12 and 24 July. In general, the M0 model over-predicts HCHO and CHOCHO concentrations by factors of 2–6 (Fig. 2e and f); and the over-estimation in G2 days is slightly higher than in G1 days. While the measurements did not find prominent diurnal variation of CHOCHO/HCHO ratios (R_{GF}), the model shows a decrease of R_{GF} from morning to noon and stable R_{GF} values in the afternoon. Higher R_{GF} are found by the model (0.075 ± 0.024) than by the measurements (0.059 ± 0.024).

4 Discussion

4.1 Modeled sources and sinks of HCHO and CHOCHO

Even though the model base-case (M0) overestimates HCHO and CHOCHO concentrations, it can provide us a hint of the relative contribution of the known NMHCs and

ACPD
13, 33013–33054, 2013

processes to the production and destruction of HCHO and CHOCHO. Figure 3 displays the production of HCHO and CHOCHO from measured NMHCs. On average, isoprene oxidation contributes most to the HCHO production (43 %), followed by the oxidation of alkenes (29 %), aromatics (15 %), and alkanes (13 %). For CHOCHO, half of its production is due to isoprene oxidation, and the other half is dominated by aromatics oxidation. The contributions of alkanes, alkenes, and ethyne to the total CHOCHO production are in total less than 10 %. The Top-10 precursor NMHCs of HCHO and CHOCHO in terms of their production rate are listed in Table 2. Compared to similar studies (e.g., Volkamer et al., 2010; Huisman et al., 2011; Washenfelder et al., 2011; MacDonald et al., 2012; Parrish et al., 2012), anthropogenic and biogenic sources contributes almost equally to the chemical formation of HCHO and CHOCHO at the BG site. However, with regard to the diurnal variation, production of HCHO and CHOCHO from anthropogenic precursors is larger than from isoprene before noon; in the afternoon, the contribution of isoprene to HCHO and CHOCHO production becomes higher than from anthropogenic NMHCs. This diurnal variation is the result of the change of airmass composition, i.e., from anthropogenically to biogenically dominated. The transition of air mass composition during daytime at the BG site has also been illustrated by Lu et al. (2012) during the analysis of the HO_x budget.

Maximum production of HCHO and CHOCHO always occurs at around noon, coinciding with the peak of OH concentrations. We investigated the production of HCHO and CHOCHO from the oxidation of NMHCs by different oxidants (i.e., OH, O_3, and NO_3). In general, OH initiated oxidation of NMHCs accounts for most of the production of HCHO and CHOCHO (> 95 %) throughout the day; ozonolysis and oxidation by NO_3 are of minor importance. Compared to HCHO, we did not find any contribution of ozonolysis of alkenes to the CHOCHO formation. With regard to the oxidation of NMHCs by NO_3, its contribution to the CHOCHO production is larger than to the HCHO production. The nighttime production of HCHO and CHOCHO from OH initiated oxidation of NMHCs results in the maximum concentration of HCHO and CHOCHO occurring in early morning hours. Without existence of OH during night, the lifetime of

ACPD
13, 33013–33054, 2013

HCHO and CHOCHO in the model is determined by dry deposition (i.e., $\tau_D = 24$ h), and the production of HCHO and CHOCHO from O_3 and NO_3 reactions is quite small. Therefore, modeled HCHO and CHOCHO concentrations during night are determined mainly by the concentrations the day before. In a model run with nighttime OH concentration fixed to zero, compared to the model M0 results, HCHO and CHOCHO show much lower concentrations during night and reach their peak concentration at a later time (≈ 2 h) (Fig. S2).

The destruction of HCHO and CHOCHO can be expressed as the sum of first order reaction rates of reaction with OH, photolysis, and dry deposition, i.e., k_d^{HCHO} and k_d^{CHOCHO}. As shown in Fig. 4, reaction with OH and photolysis are responsible for 90 % of the HCHO and CHOCHO removal during daytime. During night, HCHO and CHOCHO are removed mainly by dry deposition (60 %); the existence of nighttime OH with concentrations of around 10^6 cm^{-3} accounts for the rest. The lifetime of HCHO (reciprocal of k_d^{HCHO}) is more than 10 h during night and decreases to around 1.3 h at noon. CHOCHO has a similar lifetime as HCHO during the campaign.

The most prominent feature of HCHO and CHOCHO in the model base-case is the separation of the calculated concentrations into two groups. Different separation patterns are found for early morning (06:00–09:00 LT) and afternoon hours (12:00–18:00 LT) (Fig. 2c and d). In the afternoon, the modeled concentrations of both HCHO and CHOCHO are separated in the same way which follows the origin of the air mass arriving at the BG site. When the air mass was largely influenced by biogenic emissions (G2), the simulated HCHO and CHOCHO concentrations are more than 50 % higher than those when the air mass was from regions mainly constitute anthropogenic emissions (G1). In early morning, the simulated HCHO and CHOCHO concentrations in either G1 days (25 July for HCHO and 24 July for CHOCHO) or G2 days (12 July) can be higher than in the other days. Thus, in the following discussion, we treat the simulation results in the morning and afternoon hours separately.

The above modeled concentration difference in G1 and G2 days can be caused either by the different production or destruction rate or by both of them. Given that HCHO

ACPD
13, 33013–33054, 2013

and CHOCHO have a long lifetime (≥ 10 h) before sunrise, their concentrations during early morning hours are influenced by the production and build-up in the previous night. We checked the average production and lifetime of HCHO and CHOCHO in the period of 18:00–06:00 LT (Table 3). For both HCHO and CHOCHO, lifetime differences in the 6 days are small (< 10 %) which can not explain the > 50 % difference in the simulated concentrations. With regard to the production term, the average production rate of HCHO is around 4.4 ppb h^{-1} in the previous night of 12 and 25 July, which is 50–100 % higher than those on the other 4 days (1.9–3.2 ppb h^{-1}). Therefore, the higher simulated HCHO concentrations in the early morning of 12 and 25 July should be due to the increase of HCHO production in the previous night. However, the cause of the increase of HCHO production on 12 July is different from that on 25 July. As shown in Table 3, for 12 July, increased nighttime HCHO production are found from alkanes, alkenes and aromatics; whereas for 25 July, we see a dramatic increase of HCHO production from isoprene. For CHOCHO, its average production rate in the previous night of 12 and 24 July is 0.69 ppb h^{-1} and 0.52 ppb h^{-1}, respectively, which is much higher than in the other days (0.28–0.46 ppb h^{-1}). While the high CHOCHO production on 12 July is caused by the increase of production from aromatics, increase of production from isoprene accounts for the elevated CHOCHO production on 24 July. Similar high CHOCHO production from isoprene is found in the previous night of 25 July. Since the production from aromatics is only half of that on 24 July, the total CHOCHO production on 25 July is lower than on 24 July.

In the afternoon of the 6 cloud-free days, average HCHO and CHOCHO lifetimes are around 2 h and 1.7 h, respectively. Longer lifetimes of HCHO (3 h) and CHOCHO (2.6 h) are found on 13 July, which is due to the lower OH concentrations and photolysis frequencies. Besides 13 July, the difference of lifetimes between different days is below 30 %, with slightly lower values in G1 days than in G2 days. In G2 days, the average production rates of HCHO and CHOCHO in the afternoon are about 15 ppb h^{-1} and 1.2 ppb h^{-1}, respectively. These values are in general 50 % higher than those in G1 days (Table 3). Referring to the HCHO and CHOCHO production from different NMHC

ACPD
13, 33013–33054, 2013

in Table 3, it is clear that the enhanced production from isoprene oxidation is the major reason for the increase of the total production. Therefore, the longer lifetime as well as the increased production from isoprene lead to higher simulated HCHO and CHOCHO concentrations in G2 days than in G1 days.

For each NMHC, the change of its contribution to the total production of HCHO and CHOCHO is the result of the change of turnover rates of OH + NMHC and its follow-up reactions. This means the production of HCHO and CHOCHO depends not only on the precursor NMHC concentrations but also on the OH levels. For example, in afternoon hours, while the average OH concentrations in G2 days were similar or slightly lower than those in G1 days, significantly higher isoprene concentrations were observed in G2 days (Table 3). This caused a net increase of the turnover of OH + isoprene reaction and therefore an increased production of HCHO and CHOCHO. Moreover, the NO concentration also has an impact on the production of HCHO and CHOCHO, because the NO level determines the conversion of RO_2 to RO which finally produces HCHO and CHOCHO. At low-NO, $RO_2 + HO_2$ reaction forming hydroperoxides competes with RO_2 + NO. A sensitivity run of the M0 model shows that during low-NO_x periods (12:00–18:00 LT) a 1 % increase of the NO concentration results in an increase of modeled HCHO and CHOCHO concentration by 0.25 % and 0.1 %, respectively. The dependence of CHOCHO production on NO has also been identified by Fu et al. (2008) for the low-NO_x regime in a global model.

Compared to the situation during G2 days, the higher HCHO and CHOCHO production due to isoprene oxidation in the afternoon of G1 days could be caused by the deviation from the steady-state in the model. As illustrated by Lou et al. (2010), the modeled total OH reactivity (k_{OH}) is about 50 % higher than the measured values in the afternoon of 13, 24, and 25 July. They explain this discrepancy as a result of a strong isoprene emission at the north of the BG site. It is most likely that the air mass with freshly emitted isoprene was not fully photochemically degraded when it was detected. Here, we checked this effect by running the model M0 with different τ_D values (model MS6 in Table S2). The parameter τ_D can be used as a scale of the flushing-out speed of

ACPD
13, 33013–33054, 2013

species included in the model. The shorter the τ_D, the faster the flushing out, resulting in less reaction time Δt (i.e., similar to the photochemical age as used by Fried et al., 2011) and less oxidation products of primary emitted NMHCs. When $\tau_D = 24$ h, good agreement between modeled and measured k_{OH} is found in most periods during the campaign. However, on 13, 24, and 25 July, the value of τ_D during daytime needs to be reduced to 3 h to let the modeled k_{OH} match the measured k_{OH} (Fig. S6), indicating the shorter photochemical age of the measured air mass in these than in the other time periods.

4.2 Influences on the CHOCHO to HCHO ratio

As illustrated by Vrekoussis et al. (2010) and DiGangi et al. (2012), the CHOCHO to HCHO ratio (R_{GF}) can be used as an indicator of anthropogenic or biogenic impact on photochemistry. In the 6 cloud-free days during the PRIDE-PRD2006 campaign, the average value of measured and modeled (model M0) R_{GF} is 0.059 ± 0.024 and 0.075 ± 0.035, respectively. While HCHO and CHOCHO are mostly photochemically formed, direct emissions can contribute additionally to ambient HCHO concentrations (Garcia et al., 2006). This would lead to a decease of R_{GF}. Due to the lack of information on the primary HCHO sources for areas around the BG site, HCHO emission were not included in our model. However, in the early morning of 13, 24, and 25 July, when combustion events were prevailing in the surrounding areas of the BG site, we saw high HCHO concentrations and low R_{GF} (≈ 0.03). So, there is a possibility that some HCHO primary sources existed in the surrounding area, which causes the discrepancy between modeled and measured R_{GF}.

On the other hand, the model M0 can be used to investigate the influence of different chemical processes on the variation of R_{GF}. Given the similarity of the photochemical processes of HCHO and CHOCHO, R_{GF} shows little sensitivity on the total NMHC reactivities (k_{OH}^{TNMHC}). R_{GF} remains almost the same after decreasing k_{OH}^{TNMHC} in the model to half of the measured values. However, R_{GF} depends on the OH level. Decrease of OH concentration by 50 % results in an average decrease of R_{GF} by 20 %. Looking at

ACPD
13, 33013–33054, 2013

the diurnal variation of modeled R_{GF} (Fig. 5), an increase of R_{GF} is found since late afternoon until next early morning; and a sharp decrease of R_{GF} is identified shortly after sunrise. This diurnal variation follows the diurnal variation of NO_x concentrations and of the contribution of aromatics to the total NMHC reactivities ($k_{OH}^{Aromatics}/k_{OH}^{TNMHC}$), but is opposite to that of the contribution of isoprene to the total NMHC reactivities ($k_{OH}^{Isoprene}/k_{OH}^{TNMHC}$), indicating a positive (negative) impact of anthropogenic (biogenic) emissions on R_{GF}. A similar phenomenon was observed by DiGangi et al. (2012) at a rural site in the USA.

R_{GF} is determined by the relative strength of production and destruction of HCHO and CHOCHO. When the system is in steady-state, R_{GF} can be expressed as

$$R_{GF} = \frac{[CHOCHO]}{[HCHO]} = \frac{P_{CHOCHO}}{P_{HCHO}} \cdot \frac{k_d^{HCHO}}{k_d^{CHOCHO}} \quad (1)$$

Given a certain OH concentration, photolysis frequencies, and deposition rate, k_d^{HCHO}/k_d^{CHOCHO} is well defined and R_{GF} depends on P_{CHOCHO}/P_{HCHO}. P_{CHOCHO}/P_{HCHO} is largely influenced by NMHC composition of the investigated air mass. In the model M0, P_{CHOCHO}/P_{HCHO} of aromatic compounds (e.g., benzene, toluene, *m*,*p*-xylene) are more than 3 times larger than that of isoprene. The P_{CHOCHO}/P_{HCHO} of alkanes and alkenes are even smaller than that of isoprene, due to the little contribution of alkanes and alkenes to the CHOCHO production. Therefore, higher R_{GF} can be expected when NMHC is dominated by aromatics. Besides the NMHC composition, NO_x levels can also influence the R_{GF} since HCHO and CHOCHO have different sensitivities to the change of NO_x concentrations. When the NO concentration in the model is increased, a larger concentration increase is found for HCHO than for CHOCHO leading to a decrease of R_{GF}. The sensitivity of R_{GF} to NO is low and high in high- and low- NO regimes, respectively. An increase of NO concentration by 1 % results in a decrease of R_{GF} by 0–0.2 %. In contrast to NO, an increases of NO_2 causes an increase of R_{GF}. This is because, compared to HCHO, the modeled CHOCHO is more sensitive to NO_2.

ACPD
13, 33013–33054, 2013

Change of NO_2 concentrations can have an influence on OH (via $OH + NO_2$) and NO_3 concentrations. Since the OH concentration in the model is constrained to the measurements, CHOCHO and HCHO formation through OH initiated NMHC degradations will only be marginally affected when the NO_2 concentration is increased/decreased. Since the NO_3 reactions have different contribution to the HCHO and CHOCHO production (Sect. 4.1), increase of the modeled NO_3 concentration as a result of the increase of NO_2 can cause the change of R_{GF}. It is found that the change of R_{GF} ranges from 0 to 0.3 % when the NO_2 concentration is changed by 1 %; the lower the NO_2 concentration, the higher the sensitivity of R_{GF} to NO_2.

Based on above analysis, the modeled diurnal variation of R_{GF} can be explained by the existence of nighttime OH, by the change of NMHC composition, and by the NO_x concentration. During night, the existence of significant amounts of OH radicals made the OH + NMHC reactions the major pathway of HCHO and CHOCHO formation. The increase of R_{GF} after sunset is then the result of the increase of $k_{OH}^{Aromatics}/k_{OH}^{TNMHC}$ and of the NO_2 concentration; and the slowing down of the R_{GF} increase is caused by the occurrence of high NO concentrations later on. Around sunrise, due to the decrease of $k_{OH}^{Aromatics}/k_{OH}^{TNMHC}$ and of the NO_x concentration, and the earlier occurrence of CHOCHO photolysis (compared to HCHO, the absorption cross section of CHOCHO extends more to the visible wavelength range), the decrease of P_{CHOCHO}/P_{HCHO} and of k_d^{HCHO}/k_d^{CHOCHO} lead to the decrease of R_{GF} in the model. When setting the nighttime OH concentration to zero, modeled HCHO and CHOCHO concentrations during night are then mainly determined by their production in the previous afternoon which are mostly determined through isoprene oxidation (Sect. 4.1). As a result, modeled R_{GF} during night are as low as those during the previous afternoon when total NMHC reactivity was dominated by isoprene.

By analyzing satellite measurement results, Vrekoussis et al. (2010) concluded that high R_{GF} can represent regions strongly influenced by biogenic emissions. However, based on the in-situ observations, DiGangi et al. (2012) found that the anthropogenic emissions have positive impact on R_{GF}. Our model study at the BG site indicate that

ACPD
13, 33013–33054, 2013

the influence of anthropogenic emissions on R_{GF} is rather complicated. On the one hand, emissions of aromatics and NO_2 can contribute to the increase of R_{GF}. On the other, emitted NO and HCHO can lead to a decrease of R_{GF}. For example, compared to the period of 12:00–18:00 LT on 21 July, although the contribution of aromatics to k_{OH}^{TNMHC} is lower than on 24 July, the lower NO and higher NO_2 concentrations during 24 July caused higher modeled R_{GF}.

4.3 Possible missing sinks of HCHO and CHOCHO

Compared to the model base-case (M0) results, our measurements at the BG site show much lower concentrations of HCHO and CHOCHO which can not be explained by the uncertainties of model and measurements. Moreover, observed concentrations in the afternoon hours do not separate into different groups. To identify the explanation for these discrepancies, we performed a number of sensitivity model runs (Tables 1 and S2). Given the direct emissions of HCHO and CHOCHO are not considered in the model, periods which are under the influence of local emissions (i.e., early morning of 13, 24, and 25 July) are excluded from the analysis in this section.

As described in Sect. 4.1, the simulated HCHO and CHOCHO concentrations in the model are determined by their production and destruction processes. The employed box model could inherently overestimate the yield of HCHO and CHOCHO in the oxidation of different NMHCs. In the model M0, isoprene, alkenes and aromatics are the major precursors of HCHO and CHOCHO (Fig. 3). Firstly, when strong emission sources of these NMHCs exist in the nearby area, the model might cause an overestimation of secondary products. Secondly, HCHO and CHOCHO concentrations derived from MAX-DOAS measurements represent the average value over a certain horizontal and vertical space. During the 6 cloud free days, as estimated from the MAX-DOAS measured boundary layer height (BLH) and the visibility inside the boundary layer, the horizontal and vertical extension of the observation volume were both within ≈ 2 km (Li et al., 2010). If the air mass in this volume was not well mixed, different HCHO and

ACPD
13, 33013–33054, 2013

CHOCHO production rates compared to the rates calculated from the locally measured OH, NMHCs, etc. would be the consequence.

Since HCHO and CHOCHO are mainly coming from the reaction of OH with NMHCs, the above effects can be tested through the sensitivity of the modeled HCHO and CHOCHO on: (1) different τ_D values (i.e., flushing-out of species in the model), (2) different OH and NMHC concentrations. We already showed that when the BG site was influence by strong emissions on 13, 24, and 25 July, τ_D needs to be reduced to 3 h to match the modeled to the measured k_{OH} (Sect. 4.1). In this condition, modeled HCHO and CHOCHO concentrations decrease by 85 % of the values in the model M0 (Fig. S6). Decrease of OH concentration by 20 % can result in a maximum decrease of modeled HCHO and CHOCHO concentration by 16 % and 20 %, respectively. The reconciliation between modeled and measured HCHO (CHOCHO) concentration would require OH concentration to be decreased to < 30 % of the measured value (Fig. S2). Similar sensitivity results are found for the NMHC concentrations (Fig. S3). Within ≈ 2 km along the MAX-DOAS viewing direction, the land is covered homogeneously by trees. It is unlikely that OH or NMHC concentrations differ by a factor of 2–3 from the local measurements. However, it is possible that some short-lived NMHCs have strong vertical gradient due to vertical mixing. At around noon, the typical mixing time for a species to be well-mixed in the boundary layer is about 15 min (c.f. Stull, 1988). Given the noontime OH concentration of 1.4×10^7 cm^{-3}, this mixing time is longer than the lifetime of isoprene (≈ 10 min) but is much shorter than the lifetime of aromatics and other alkenes at the BG site. Therefore, isoprene emitted at ground level could not be well-mixed in the boundary layer within its lifetime. Assuming a vertical exponential decay of the isoprene concentration in the boundary layer and using the measured noontime BLH of around 2 km, the effective average isoprene concentration in the boundary layer is estimated to be only 52 % of the measured value at ground (i.e., the value used in the model M0). For the time period when convective mixing is strong, i.e., 08:00–16:00 LT, we reduced isoprene concentration in the model to 52 % of the measured value. Compared to the model M0, it results in an average decrease of mod-

ACPD
13, 33013–33054, 2013

eled HCHO and CHOCHO concentration by 15 % (Fig. S3). The decrease is larger (up to 35 %) in days when the BG site was influenced by strong isoprene emissions (i.e., 13, 24, and 25 July).

Together with the formation of HCHO and CHOCHO, hydroperoxides (e.g., H_2O_2, CH_3OOH) and peroxyacyl nitrates (PANs) are produced in the oxidation of NMHCs. So, using these measurement results as additional constraints in the model, the prediction of NMHC oxidation processes can be improved (Kormann et al., 2003). It is found that the model run with measured H_2O_2 and CH_3OOH gives nearly the same HCHO and CHOCHO concentrations as in the model base-case (Fig. S4). Including measured PANs in the model can only lead to a maximum reduction of modeled HCHO concentration by 30 % (Fig. S5). Modeled HCHO and CHOCHO seem not to be sensitive to the change of hydroperoxides and PANs abundance.

By using the modified τ_D values and isoprene concentrations in the model, and including PANs measurements as additional model constraints (model M1), the modeled HCHO (CHOCHO) concentrations during daytime (06:00–18:00 LT) decrease by 67 % (60 %) of the values in the model M0 for 13, 24, and 25 July, and by 31 % (13 %) for 12, 20, and 21 July. Given the uncertainties of model and measurements, the model results agree with the measurements of 13, 24, and 25 July, but are twice as high as the measured values for 12, 20, and 21 July (Fig. 6). Therefore, the uncertainties of the source terms of HCHO and CHOCHO in the model can only partly explain the discrepancy between modeled and measured concentrations. So, HCHO and CHOCHO sink terms are most likely underestimated by the model.

The missing HCHO and CHOCHO sinks can originate either from the range of the existing HCHO and CHOCHO destruction terms in the model (i.e., reaction with OH, photolysis, and dry deposition), or from horizontal advection, vertical dilution, or loss on aerosol surfaces which are not considered in the model.

We showed above that the sensitivity of modeled HCHO and CHOCHO on the change of OH concentration can not explain the overestimation of HCHO and CHOCHO concentration. Since all the days mentioned in this paper had clear-sky

ACPD
13, 33013–33054, 2013

conditions, the photolysis frequency measurements were representative enough for the entire MAX-DOAS observation volume. Given that the photolysis frequency measurements have an accuracy of 10 %, they can only have a minor influence on the overestimation.

Dry deposition of trace gases was included in the model by a constant lifetime τ_D = 24 h, which corresponds to a deposition velocity of 1.6 cm s^{-1} when taking the average measured daytime BLH of 1.4 km. The reported deposition velocities of HCHO and CHOCHO are 0.05–1 cm s^{-1} (Stickler et al., 2006) and 0.15–0.3 cm s^{-1} (c.f. Washenfelder et al., 2011), respectively. Though the average loss of HCHO and CHOCHO through dry deposition in the model M0 is faster than reported, it does not take the diurnal variation of boundary layer into account. During night, assuming a BLH of 100 m, a deposition velocity of 1 cm s^{-1} results in a lifetime of 2.8 h which is an order of magnitude shorter than the τ_D of 24 h. This means the loss of HCHO and CHOCHO during night should be faster than the model M0 predicted. Based on model M1, we replaced the constant τ_D of HCHO (CHOCHO) by a time dependent lifetime calculated from the measured BLH (assume nighttime value of 100 m) and a deposition velocity of 1 cm s^{-1} (0.3 cm s^{-1}) (model M2). As shown in Fig. 6, for morning hours (06:00–10:00 LT), the calculated HCHO and CHOCHO concentrations by model M2 decrease by 34 % and 16 % of the values by model M1, respectively. However, the influence of dry deposition on the modeled HCHO and CHOCHO is marginal during the afternoon.

If the air mass detected by MAX-DOAS was inhomogeneously mixed, the HCHO and CHOCHO concentrations calculated from locally measured OH, NMHCs, etc. could be different from that at other points. This will result in HCHO and CHOCHO concentration gradients, and lead to HCHO and CHOCHO transport through horizontal advection. During daytime, considering the short lifetime of HCHO and CHOCHO ($\approx$ 1.5 h), the low wind speed ($\approx$ 2 m s^{-1}) at the BG site, and the homogeneous type of land usage along the MAX-DOAS viewing direction, horizontal advection might have only a minor influence on the HCHO and CHOCHO simulation.

ACPD
13, 33013–33054, 2013

With regard to the vertical dilution which is caused by the lift of the boundary layer during sunrise, we can estimate the dilution rate constant (k_{dilu}) from the decay of the measured black carbon concentrations. During the campaign, the black carbon concentration usually experienced a fast decrease around sunrise (i.e., 06:00–10:00 LT) and showed stable values after 11:00 LT until sunset. The diurnal variation of the black carbon concentration indicates an efficient vertical dilution in the period of 06:00–10:00 LT, and a well mixed boundary layer since 11:00 LT. In the 6 modeling days, the calculated k_{dilu} ranges from 0.2 to 0.61 h^{-1} with an average value of 0.41 h^{-1}. Assuming a constant k_{dilu} of 0.41 h^{-1}, we applied the removal of all species by vertical dilution for the time period of 06:00–10:00 LT in the model M2 (i.e., model M3). Compared to model M2, significant decrease (by ≈ 40 %) of modeled HCHO and CHOCHO concentrations can be identified during morning hours (Fig. 6).

In addition to the modification of source terms of HCHO and CHOCHO in the model, including vertical dilution and modified dry deposition (model M3) results in reasonable agreement between modeled and measured HCHO and CHOCHO concentrations in most of the time during the 6 cloud-free days (Fig. 6). However, during early morning hours (06:00–09:00 LT), the modeled CHOCHO concentrations are still significantly higher than the measured values. For days without the influence of direct emission in the morning (i.e., 12, 20, and 21 July), the modeled HCHO concentrations are also higher than the measured values.

Laboratory and field studies indicate that HCHO and CHOCHO in the gas phase can be lost on aerosols through heterogeneous uptake processes (Volkamer et al., 2007; Wang et al., 2010; Li et al., 2011; Washenfelder et al., 2011). This uptake process has been shown to be related to the acidity (Jayne et al., 1996; Liggio et al., 2005) or the ionic strength (Kroll et al., 2005) of aerosols. Using an online Aerosol Inorganics Model (AIM, Model II) (http://www.aim.env.uea.ac.uk/aim/model2/model2a.php) and the method described by Zhang et al. (2007), we estimated H^+ activity a_{H^+} and ionic strength within the aqueous particle phase from AMS measurements of NH_4^+, SO_4^{2-}, NO_3^-, and Cl^- in PM_1. During the daytime of the 6 cloud free days, the average

ACPD
13, 33013–33054, 2013

value of the calculated a_{H^+} was 1.47×10^{-2} mol L^{-1} (corresponding to a pH value of 1.8), indicating high aerosol acidity at the BG site. Given the high aerosol concentrations in the early morning hours (Fig. 1d), we investigated the sensitivity of modeled HCHO and CHOCHO concentrations on heterogeneous uptake processes (i.e., model M4). Using an uptake coefficient of 10^{-3} as indicated by laboratory and field studies (Jayne et al., 1996; Liggio et al., 2005; Volkamer et al., 2007), the calculated CHOCHO concentration by model M4 decrease significantly (by ≈ 70 %) from that by model M3 for the early morning hours. In the afternoon, due to decreased aerosol concentration, the influence of the uptake by aerosols on the modeled CHOCHO concentrations becomes small. Compared to the model M3, the model M4 provides better agreement between modeled and measured HCHO and CHOCHO concentrations (Fig. 6). Under tropospheric conditions, while the uptake coefficient of 10^{-3} can be realistic for CHOCHO, it remains large uncertainty for HCHO. The value of 10^{-3} used in the model M4 for HCHO is estimated from laboratory studies representing typical conditions in the upper troposphere or in the stratosphere (i.e., low temperature and high aerosol acidity) (Jayne et al., 1996). During experiments performed under tropospheric conditions by Kroll et al. (2005), no uptake of HCHO by aerosols was observed. However, some laboratory (Sassine et al., 2010; Li et al., 2011) and field (Wang et al., 2010) studies identified loss of HCHO on tropospheric aerosols under certain conditions. Therefore, it is possible that the use of 10^{-3} as the HCHO uptake coefficient could not well represent the condition at the BG site.

Table 4 summarizes the relative changes of modeled HCHO and CHOCHO concentrations by adding additional mechanisms in the model M0 (i.e., M1–M4). By including possible missing considerations of production and destruction terms (i.e., model M4), the modeled HCHO and CHOCHO concentrations during daytime (06:00–18:00 LT) decrease by ≈ 80 % of the values predicted by the model M0. On average, the production terms (i.e., deviation from steady-state, vertical transport of isoprene) and the uptake by aerosols have the largest effect (≈ 50 %) on the concentration decrease, followed

ACPD
13, 33013–33054, 2013

by vertical dilution (≈ 30 %) and deposition (≈ 15 %). Increased influence of vertical dilution and deposition on the concentration decrease can be found for morning hours.

In addition to the chemical mechanisms discussed in Section 4.2, additional processes included in the model M1–M4 also influence the CHOCHO to HCHO ratio (R_{GF}). As shown in Table 4 and Fig. 6, during daytime, the modeled R_{GF} by the model M4 increase by 30 % of the values by the model M0. Larger increase of R_{GF} can be found during night, mainly caused by the faster removal of HCHO by dry deposition than that of CHOCHO. Different from other processes, vertical dilution generally causes small decrease of R_{GF}.

5 Summary and conclusion

HCHO and CHOCHO are trace gases produced through the oxidation of NMHCs. High vertical column densities of HCHO and CHOCHO have been observed by satellite measurements for the Pearl River Delta (PRD) region in southern China, indicating the existence of high photochemical reactivity. However, investigations on the sources and sinks of HCHO and CHOCHO in PRD are rather limited. During the PRIDE-PRD2006 campaign, MAX-DOAS observations of HCHO and CHOCHO together with measurements of HO_x radicals, trace gases, aerosols, and meteorological parameters were performed at a semi-rural site Back Garden (BG) in PRD. Using these measurement results and a box model, we investigated production and destruction processes of HCHO and CHOCHO for 6 cloud-free days during the campaign.

The production of HCHO and CHOCHO at the BG site took place under the combined influence of anthropogenic and biogenic emissions. OH initiated oxidation of isoprene accounts for nearly half of the HCHO and CHOCHO formation, with increased contribution in the afternoon. The anthropogenic source of HCHO includes the degradation of alkenes (29 %), aromatics (15 %), and alkanes (13 %). Besides isoprene, most of the CHOCHO production is due to the oxidation of aromatics (41 %). While the ozonolysis of alkenes contributes to the formation of HCHO, some CHOCHO is

ACPD
13, 33013–33054, 2013

formed through the oxidation of NMHCs by NO_3 radicals. However, compared to the OH initiated oxidation of NMHCs, ozonolysis of alkenes and NO_3 initiated NMHCs degradations are of minor importance in terms of the HCHO and CHOCHO production. The existence of OH radicals at night results in the maximum HCHO and CHOCHO concentrations occurred in the early morning, which is different from the observations in the other places in the world.

Our model simulations indicate that the CHOCHO to HCHO ratio at the BG site is influenced not only by the NMHC composition but also by the concentration levels of OH and NO_x. Higher R_{GF} exist for higher aromatic contents to the total NMHCs, for higher OH and NO_2 but lower NO concentrations. Moreover, processes like vertical transport/dilution, dry deposition, and uptake by aerosols can also influence the CHOCHO to HCHO ratio. The complicate dependence of R_{GF} on NMHCs, OH, NO_x, and other physical/chemical processes suggest to be careful when using R_{GF} as an indicator of anthropogenic or biogenic emissions.

Compared to the measurements, the box model overestimates the HCHO and CHOCHO concentrations by a factor of 2–5. This discrepancy is to a large extent (> 70 %) caused by the missing consideration of fresh emissions, vertical transport of precursor NMHCs, and uptake of HCHO and CHOCHO by aerosols in the model. Insufficient treatments of dry deposition of HCHO and CHOCHO and of vertical dilution of all species in the model account for the rest 30 % discrepancy. Our analysis indicates that, in addition to chemical mechanisms, the atmospheric physical processes (e.g., transport, dilution, dry deposition) have to be well considered for a box model predicting HCHO and CHOCHO concentrations.

Supplementary material related to this article is available online at http://www.atmos-chem-phys-discuss.net/13/33013/2013/acpd-13-33013-2013-supplement.pdf.

ACPD
13, 33013–33054, 2013

Acknowledgements. This work was supported by China National Basic Research and Development Program 2002CB410801, National High Technology Research and Development Program of China (863 Program) 2006AA06A301, and National Natural Science Foundation of China (21190052)

The service charges for this open access publication have been covered by a Research Centre of the Helmholtz Association.

References

Choi, W., Faloona, I. C., Bouvier-Brown, N. C., McKay, M., Goldstein, A. H., Mao, J., Brune, W. H., LaFranchi, B. W., Cohen, R. C., Wolfe, G. M., Thornton, J. A., Sonnenfroh, D. M., and Millet, D. B.: Observations of elevated formaldehyde over a forest canopy suggest missing sources from rapid oxidation of arboreal hydrocarbons, Atmos. Chem. Phys., 10, 8761–8781, doi:10.5194/acp-10-8761-2010, 2010. 33016

DiGangi, J. P., Boyle, E. S., Karl, T., Harley, P., Turnipseed, A., Kim, S., Cantrell, C., Maudlin III, R. L., Zheng, W., Flocke, F., Hall, S. R., Ullmann, K., Nakashima, Y., Paul, J. B., Wolfe, G. M., Desai, A. R., Kajii, Y., Guenther, A., and Keutsch, F. N.: First direct measurements of formaldehyde flux via eddy covariance: implications for missing in-canopy formaldehyde sources, Atmos. Chem. Phys., 11, 10565–10578, doi:10.5194/acp-11-10565-2011, 2011. 33015

DiGangi, J. P., Henry, S. B., Kammrath, A., Boyle, E. S., Kaser, L., Schnitzhofer, R., Graus, M., Turnipseed, A., Park, J-H., Weber, R. J., Hornbrook, R. S., Cantrell, C. A., Maudlin III, R. L., Kim, S., Nakashima, Y., Wolfe, G. M., Kajii, Y., Apel, E.C., Goldstein, A. H., Guenther, A., Karl, T., Hansel, A., and Keutsch, F. N.: Observations of glyoxal and formaldehyde as metrics for the anthropogenic impact on rural photochemistry, Atmos. Chem. Phys., 12, 9529–9543, doi:10.5194/acp-12-9529-2012, 2012. 33016, 33017, 33027, 33028, 33029

Finlayson-Pitts, B. J. and Pitts, J. N.: Chemistry of the Upper and Lower Atmosphere – Theory, Experiments and Applications, 1st edn., Academic Press, San Diego, 2000. 33015

Fortems-Cheiney, A., Chevallier, F., Pison, I., Bousquet, P., Saunois, M., Szopa, S., Cressot, C., Kurosu, T. P., Chance, K., and Fried, A.: The formaldehyde budget as seen by a global-scale

ACPD
13, 33013–33054, 2013

multi-constraint and multi-species inversion system, Atmos. Chem. Phys., 12, 6699–6721, doi:10.5194/acp-12-6699-2012, 2012. 33015

Fried, A., Crawford, J., Olson, J., Walega, J., Potter, W., Wert, B., Jordan, C., Anderson, B., Shetter, R., Lefer, B., Blake, D., Blake, N., Meinardi, S., Heikes, B., O'Sullivan, D., Snow, J., Fuelberg, H., Kiley, C. M., Sandholm, S., Tan, D., Sachse, G., Singh, H., Faloona, I., Harward, C. N., and Carmichael, G. R.: Airborne tunable diode laser measurements of formaldehyde during TRACE-P: distributions and box model comparisons, J. Geophys. Res., 108, 8798, doi:10.1029/2003jd003451, 2003a. 33015, 33016

Fried, A., Wang, Y., Cantrell, C., Wert, B., Walega, J., Ridley, B., Atlas, E., Shetter, R., Lefer, B., Coffey, M. T., Hannigan, J., Blake, D., Blake, N., Meinardi, S., Talbot, B., Dibb, J., Scheuer, E., Wingenter, O., Snow, J., Heikes, B., and Ehhalt, D.: Tunable diode laser measurements of formaldehyde during the TOPSE 2000 study: distributions, trends, and model comparisons, J. Geophys. Res., 108, D4, 8365, doi:10.1029/2002jd002208, 2003b. 33016

Fried, A., Cantrell, C., Olson, J., Crawford, J. H., Weibring, P., Walega, J., Richter, D., Junkermann, W., Volkamer, R., Sinreich, R., Heikes, B. G., O'Sullivan, D., Blake, D. R., Blake, N., Meinardi, S., Apel, E., Weinheimer, A., Knapp, D., Perring, A., Cohen, R. C., Fuelberg, H., Shetter, R. E., Hall, S. R., Ullmann, K., Brune, W. H., Mao, J., Ren, X., Huey, L. G., Singh, H. B., Hair, J. W., Riemer, D., Diskin, G., and Sachse, G.: Detailed comparisons of airborne formaldehyde measurements with box models during the 2006 INTEX-B and MILAGRO campaigns: potential evidence for significant impacts of unmeasured and multi-generation volatile organic carbon compounds, Atmos. Chem. Phys., 11, 11867–11894, doi:10.5194/acp-11-11867-2011, 2011. 33016, 33027

Fu, T.-M., Jacob, D. J., Wittrock, F., Burrows, J. P., Vrekoussis, M., and Henze, D. K.: Global budgets of atmospheric glyoxal and methylglyoxal, and implications for formation of secondary organic aerosols, J. Geophys. Res., 113, D15303, doi:10.1029/2007JD009505, 2008. 33016, 33026

Garcia, A. R., Volkamer, R., Molina, L. T., Molina, M. J., Samuelson, J., Mellqvist, J., Galle, B., Herndon, S. C., and Kolb, C. E.: Separation of emitted and photochemical formaldehyde in Mexico City using a statistical analysis and a new pair of gas-phase tracers, Atmos. Chem. Phys., 6, 4545–4557, doi:10.5194/acp-6-4545-2006, 2006. 33027

Hofzumahaus, A., Rohrer, F., Lu, K., Bohn, B., Brauers, T., Chang, C.-C., Fuchs, H., Holland, F., Kita, K., Kondo, Y., Li, X., Lou, S., Shao, M., Zeng, L., Wahner, A., and

ACPD
13, 33013–33054, 2013

Zhang, Y.: Amplified trace gas removal in the troposphere, Science, 324, 1702–1704, doi:10.1126/science.1164566, 2009. 33020

Hu, W. W., Hu, M., Deng, Z. Q., Xiao, R., Kondo, Y., Takegawa, N., Zhao, Y. J., Guo, S., and Zhang, Y. H.: The characteristics and origins of carbonaceous aerosol at a rural site of PRD in summer of 2006, Atmos. Chem. Phys., 12, 1811–1822, doi:10.5194/acp-12-1811-2012, 2012. 33017, 33021

Huisman, A. J., Hottle, J. R., Galloway, M. M., DiGangi, J. P., Coens, K. L., Choi, W., Faloona, I. C., Gilman, J. B., Kuster, W. C., de Gouw, J., Bouvier-Brown, N. C., Goldstein, A. H., LaFranchi, B. W., Cohen, R. C., Wolfe, G. M., Thornton, J. A., Docherty, K. S., Farmer, D. K., Cubison, M. J., Jimenez, J. L., Mao, J., Brune, W. H., and Keutsch, F. N.: Photochemical modeling of glyoxal at a rural site: observations and analysis from BEARPEX 2007, Atmos. Chem. Phys., 11, 8883–8897, doi:10.5194/acp-11-8883-2011, 2011. 33016, 33023

Jang, M. and Kamens, R. M.: Atmospheric secondary aerosol formation by heterogeneous reactions of aldehydes in the presence of a sulfuric acid aerosol catalyst, Environ. Sci. Technol., 35, 4758–4766, doi:10.1021/es010790s, 2001. 33016

Jayne, J. T., Worsnop, D. R., Kolb, C. E., Swartz, E., and Davidovits, P.: Uptake of gas-phase formaldehyde by aqueous acid surfaces, J. Phys. Chem., 100, 8015–8022, doi:10.1021/jp953196b, 1996. 33015, 33034, 33035

Kormann, R., Fischer, H., de Reus, M., Lawrence, M., Brühl, Ch., von Kuhlmann, R., Holzinger, R., Williams, J., Lelieveld, J., Warneke, C., de Gouw, J., Heland, J., Ziereis, H., and Schlager, H.: Formaldehyde over the eastern Mediterranean during MINOS: Comparison of airborne in-situ measurements with 3D-model results, Atmos. Chem. Phys., 3, 851–861, doi:10.5194/acp-3-851-2003, 2003. 33016, 33032

Kroll, J. H., Ng, N. L., Murphy, S. M., Varutbangkul, V., Flagan, R. C., and Seinfeld, J. H.: Chamber studies of secondary organic aerosol growth by reactive uptake of simple carbonyl compounds, J. Geophys. Res., 110, D23207, doi:10.1029/2005jd006004, 2005. 33015, 33017, 33034, 33035

Lee, M., Heikes, B. G., Jacob, D. J., Sachse, G., and Anderson, B.: Hydrogen peroxide, organic hydroperoxide, and formaldehyde as primary pollutants from biomass burning, J. Geophys. Res., 102, 1301–1309, doi:10.1029/96jd01709, 1997. 33015

Li, X., Brauers, T., Shao, M., Garland, R. M., Wagner, T., Deutschmann, T., and Wahner, A.: MAX-DOAS measurements in southern China: retrieval of aerosol extinctions and validation

ACPD
13, 33013–33054, 2013

using ground-based in-situ data, Atmos. Chem. Phys., 10, 2079–2089, doi:10.5194/acp-10-2079-2010, 2010. 33030

Li, X., Brauers, T., Häseler, R., Bohn, B., Fuchs, H., Hofzumahaus, A., Holland, F., Lou, S., Lu, K. D., Rohrer, F., Hu, M., Zeng, L. M., Zhang, Y. H., Garland, R. M., Su, H., Nowak, A., Wiedensohler, A., Takegawa, N., Shao, M., and Wahner, A.: Exploring the atmospheric chemistry of nitrous acid (HONO) at a rural site in Southern China, Atmos. Chem. Phys., 12, 1497–1513, doi:10.5194/acp-12-1497-2012, 2012. 33020

Li, X., Brauers, T., Hofzumahaus, A., Lu, K., Li, Y. P., Shao, M., Wagner, T., and Wahner, A.: MAX-DOAS measurements of NO_2, HCHO and CHOCHO at a rural site in Southern China, Atmos. Chem. Phys., 13, 2133–2151, doi:10.5194/acp-13-2133-2013, 2013. 33017, 33018

Li, Z., Schwier, A. N., Sareen, N., and McNeill, V. F.: Reactive processing of formaldehyde and acetaldehyde in aqueous aerosol mimics: surface tension depression and secondary organic products, Atmos. Chem. Phys., 11, 11617–11629, doi:10.5194/acp-11-11617-2011, 2011. 33015, 33034, 33035

Liggio, J., Li, S.-M., and McLaren, R.: Reactive uptake of glyoxal by particulate matter, J. Geophys. Res., 110, D10304, doi:10.1029/2004jd005113, 2005. 33017, 33034, 33035

Liu, X., Cheng, Y., Zhang, Y., Jung, J., Sugimoto, N., Chang, S.-Y., Kim, Y. J., Fan, S., and Zeng, L.: Influences of relative humidity and particle chemical composition on aerosol scattering properties during the 2006 PRD campaign, Atmos. Environ., 42, 1525–1536, doi:10.1016/j.atmosenv.2007.10.077, 2008. 33049

Liu, Z., Wang, Y., Vrekoussis, M., Richter, A., Wittrock, F., Burrows, J. P., Shao, M., Chang, C.-C., Liu, S.-C., Wang, H., and Chen, C.: Exploring the missing source of glyoxal (CHOCHO) over China, Geophys. Res. Lett., 39, L10812, doi:10.1029/2012GL051645, 2012. 33016

Lou, S., Holland, F., Rohrer, F., Lu, K., Bohn, B., Brauers, T., Chang, C.C., Fuchs, H., Häseler, R., Kita, K., Kondo, Y., Li, X., Shao, M., Zeng, L., Wahner, A., Zhang, Y., Wang, W., and Hofzumahaus, A.: Atmospheric OH reactivities in the Pearl River Delta – China in summer 2006: measurement and model results, Atmos. Chem. Phys., 10, 11243–11260, doi:10.5194/acp-10-11243-2010, 2010. 33017, 33026

Lu, K. D., Rohrer, F., Holland, F., Fuchs, H., Bohn, B., Brauers, T., Chang, C. C., Häseler, R., Hu, M., Kita, K., Kondo, Y., Li, X., Lou, S. R., Nehr, S., Shao, M., Zeng, L. M., Wahner, A., Zhang, Y. H., and Hofzumahaus, A.: Observation and modelling of OH and HO_2 concentrations in the Pearl River Delta 2006: a missing OH source in a VOC rich atmosphere, Atmos.

ACPD
13, 33013–33054, 2013

Chem. Phys., 12, 1541–1569, doi:10.5194/acp-12-1541-2012, 2012. 33017, 33018, 33019, 33020, 33023
MacDonald, S. M., Oetjen, H., Mahajan, A. S., Whalley, L. K., Edwards, P. M., Heard, D. E., Jones, C. E., and Plane, J. M. C.: DOAS measurements of formaldehyde and glyoxal above a south-east Asian tropical rainforest, Atmos. Chem. Phys., 12, 5949–5962, doi:10.5194/acp-12-5949-2012, 2012. 33016, 33017, 33023
Myriokefalitakis, S., Vrekoussis, M., Tsigaridis, K., Wittrock, F., Richter, A., Brühl, C., Volkamer, R., Burrows, J. P., and Kanakidou, M.: The influence of natural and anthropogenic secondary sources on the glyoxal global distribution, Atmos. Chem. Phys., 8, 4965–4981, doi:10.5194/acp-8-4965-2008, 2008. 33016
Parrish, D. D., Ryerson, T. B., Mellqvist, J., Johansson, J., Fried, A., Richter, D., Walega, J. G., Washenfelder, R. A., de Gouw, J. A., Peischl, J., Aikin, K. C., McKeen, S. A., Frost, G. J., Fehsenfeld, F. C., and Herndon, S. C.: Primary and secondary sources of formaldehyde in urban atmospheres: Houston Texas region, Atmos. Chem. Phys., 12, 3273–3288, doi:10.5194/acp-12-3273-2012, 2012. 33015, 33023
Sassine, M., Burel, L., D'Anna, B., and George, C.: Kinetics of the tropospheric formaldehyde loss onto mineral dust and urban surfaces, Atmos. Environ., 44, 5468–5475, doi:10.1016/j.atmosenv.2009.07.044, 2010. 33015, 33035
Schauer, J. J., Kleeman, M. J., Cass, G. R., and Simoneit, B. R. T.: Measurement of emissions from air pollution sources, 2. C1 through C30 organic compounds from medium duty diesel trucks, Environ. Sci. Technol., 33, 1578–1587, doi:10.1021/es980081n, 1999. 33015
Schauer, J. J., Kleeman, M. J., Cass, G. R., and Simoneit, B. R. T.: Measurement of emissions from air pollution sources, 5. C1 through C32 organic compounds from gasoline-powered motor vehicles, Environ. Sci. Technol., 36, 1169–1180, doi:10.1021/es0108077, 2002. 33015
Stavrakou, T., Müller, J.-F., De Smedt, I., Van Roozendael, M., Kanakidou, M., Vrekoussis, M., Wittrock, F., Richter, A., and Burrows, J. P.: The continental source of glyoxal estimated by the synergistic use of spaceborne measurements and inverse modelling, Atmos. Chem. Phys., 9, 8431–8446, doi:10.5194/acp-9-8431-2009, 2009. 33016
Stickler, A., Fischer, H., Williams, J., de Reus, M., Sander, R., Lawrence, M. G., Crowley, J. N., and Lelieveld, J.: Influence of summertime deep convection on formaldehyde in the middle and upper troposphere over Europe, J. Geophys. Res., 111, D14308, doi:10.1029/2005jd007001, 2006. 33033

ACPD
13, 33013–33054, 2013

Stull, R. B.: An Introduction to Boundary Layer Meteorology, Kluwer Academic Publishers, Dordrecht, the Netherlands, 1988. 33031

Tan, Y., Perri, M. J., Seitzinger, S. P., and Turpin, B. J.: Effects of precursor concentration and acidic sulfate in aqueous glyoxal-OH radical oxidation and implications for secondary organic aerosol, Environ. Sci. Technol., 43, 8105–8112, doi:10.1021/es901742f, 2009. 33017

Tie, X., Brasseur, G., Emmons, L., Horowitz, L., and Kinnison, D.: Effects of aerosols on tropospheric oxidants: a global model study, J. Geophys. Res., 106, 22931–22964, doi:10.1029/2001jd900206, 2001. 33015

Volkamer, R., San Martini, F., Molina, L. T., Salcedo, D., Jimenez, J. L., and Molina, M. J.: A missing sink for gas-phase glyoxal in Mexico City: formation of secondary organic aerosol, Geophys. Res. Lett., 34, L19807, doi:10.1029/2007gl030752, 2007. 33016, 33017, 33034, 33035

Volkamer, R., Sheehy, P., Molina, L. T., and Molina, M. J.: Oxidative capacity of the Mexico City atmosphere – Part 1: A radical source perspective, Atmos. Chem. Phys., 10, 6969–6991, doi:10.5194/acp-10-6969-2010, 2010. 33023

Vrekoussis, M., Wittrock, F., Richter, A., and Burrows, J. P.: GOME-2 observations of oxygenated VOCs: what can we learn from the ratio glyoxal to formaldehyde on a global scale?, Atmos. Chem. Phys., 10, 10145–10160, doi:10.5194/acp-10-10145-2010, 2010. 33017, 33027, 33029

Wagner, V., Schiller, C., and Fischer, H.: Formaldehyde measurements in the marine boundary layer of the Indian Ocean during the 1999 INDOEX cruise of the R/V *Ronald H. Brown*, J. Geophys. Res., 106, 28529–28538, doi:10.1029/2000jd900825, 2001. 33016

Wang, X., Gao, S., Yang, X., Chen, H., Chen, J., Zhuang, G., Surratt, J. D., Chan, M. N., and Seinfeld, J. H.: Evidence for high molecular weight nitrogen-containing organic salts in urban aerosols, Environ. Sci. Technol., 44, 4441–4446, doi:10.1021/es1001117, 2010. 33015, 33034, 33035

Washenfelder, R. A., Young, C. J., Brown, S. S., Angevine, W. M., Atlas, E. L., Blake, D. R., Bon, D. M., Cubison, M. J., de Gouw, J. A., Dusanter, S., Flynn, J., Gilman, J. B., Graus, M., Griffith, S., Grossberg, N., Hayes, P. L., Jimenez, J. L., Kuster, W. C., Lefer, B. L., Pollack, I. B., Ryerson, T. B., Stark, H., Stevens, P. S., and Trainer, M. K.: The glyoxal budget and its contribution to organic aerosol for Los Angeles, California, during CalNex 2010, J. Geophys. Res., 116, D00V02, doi:10.1029/2011JD016314, 2011. 33016, 33017, 33023, 33033, 33034

ACPD
13, 33013–33054, 2013

Wittrock, F., Richter, A., Oetjen, H., Burrows, J. P., Kanakidou, M., Myriokefalitakis, S., Volkamer, R., Beirle, S., Platt, U., and Wagner, T.: Simultaneous global observations of glyoxal and formaldehyde from space, Geophys. Res. Lett., 33, L16804, doi:10.1029/2006gl026310, 2006. 33017

Zhang, Q., Jimenez, J. L., Worsnop, D. R., and Canagaratna, M.: A case study of urban particle acidity and its influence on secondary organic aerosol, Environ. Sci. Technol., 41, 3213–3219, doi:10.1021/es061812j, 2007. 33034

Zhou, X., Lee, Y.-N., Newman, L., Chen, X., and Mopper, K.: Tropospheric formaldehyde concentration at the Mauna Loa Observatory during the Mauna Loa Observatory Photochemistry Experiment 2, J. Geophys. Res., 101, 14711–14719, doi:10.1029/95jd03226, 1996. 33015

ACPD
13, 33013–33054, 2013

Table 1. Model scenarios used in the sensitivity study of HCHO and CHOCHO simulation during the PRIDE-PRD2006 campaign.

Simulation	Mechanisms	Purpose
M0	MCM v3.2 with $\tau_D = 24$ h	Base run
M1	as M0, but (1) change τ_D to 3 h for the time period of 06:00–19:00 LT in 13, 24, and 25 July, (2) decrease isoprene concentration to 30 % of the measured value for the period of 08:00–16:00 LT, and (3) include measured PANs as model constraints	Influence of source terms
M2	as M1, but replace τ_D of HCHO and CHOCHO by $\tau_{depo.} = \frac{v_{depo.}}{BLH}$. $v_{depo.}$ is set to 1 cm s^{-1} and 0.3 cm s^{-1} for HCHO and CHOCHO, respectively.	Influence of dry deposition
M3	as M2, but add removal of all species by vertical dilution for the period of 06:00–10:00 LT, with rate constant of 0.41 h^{-1}	Influence of vertical dilution
M4	as M3, but include uptake of HCHO and CHOCHO by aerosols, i.e., $\frac{dC}{dt} = -\frac{\gamma \times S_{aw} \times v \times C^*}{4}$, with an uptake coefficient γ of 10^{-3}	Influence of heterogeneous uptake

* C, v, and γ are the gas phase concentration, mean molecular velocity, and uptake coefficient, respectively. S_{aw} is the RH corrected aerosol surface concentration.

ACPD
13, 33013–33054, 2013

Table 2. Top-10 precursor NMHCs of HCHO and CHOCHO for the 6 cloud-free days during the PRIDE-PRD2006 campaign.

NMHCs	P_{HCHO} ppb h^{-1}	%	NMHCs	P_{CHOCHO} ppb h^{-1}	%
Isoprene	3.85	43.2	Isoprene	0.37	51.5
Propene	0.97	12.8	Toluene	0.17	22.0
Ethene	0.67	8.2	Ethylbenzene	0.04	5.2
Styrene	0.24	6.1	*m*-Xylene	0.04	5.1
Methane	0.30	4.2	Ethene	0.03	4.2
m-Xylene	0.33	3.2	Benzene	0.03	4.0
1-Butene	0.17	2.5	*o*-Xylene	0.02	2.8
trans-2-Butene	0.18	2.2	Ethyne	0.02	2.4
Toluene	0.21	1.9	1,2,4-Trimethylbenzene	0.01	1.3
cis-2-Butene	0.15	1.7	*o*-Ethylbenzene	0.004	0.5

ACPD
13, 33013–33054, 2013

Table 3. Average production rates of HCHO and CHOCHO, NMHC reactivities, and radical and trace gases concentrations in the model base-case (M0) for the 6 cloud-free days during the PRIDE-PRD2006 campaign. The NMHC reactivity is defined as the product between NMHC concentration and its rate constant of reaction with OH (at 298 K and 1 atm).

Parameter	18:00 (−1 day)–06:00 LT						12:00–18:00 LT					
	12	20	21	13	24	25	12	20	21	13	24	25
	Production rate, ppb h^{-1}											
$P^{Alkanes}_{HCHO}$	0.86	0.25	0.2	0.42	0.41	0.27	2.85	1.51	0.99	1.97	1.69	1.14
$P^{Alkenes}_{HCHO}$	1.71	0.52	0.54	0.74	0.95	1.18	3.55	2.45	1.72	2.85	2.88	2.98
P^{Ethyne}_{HCHO}	–	–	–	–	–	–	–	–	–	–	–	–
$P^{Aromatics}_{HCHO}$	1.15	0.4	0.28	0.37	0.5	0.55	1.05	0.68	0.34	0.93	1.22	0.66
$P^{Isoprene}_{HCHO}$	0.68	0.76	0.88	0.73	1.34	2.48	4.82	5.36	3.82	8.79	10.25	11.92
P^{Total}_{HCHO}	4.4	1.93	1.9	2.26	3.20	4.47	12.27	10	6.87	14.54	16.04	16.7
$P^{Alkanes}_{CHOCHO}$	0.01	–	–	0.01	–	–	0.03	0.01	0.01	0.01	0.03	–
$P^{Alkenes}_{CHOCHO}$	0.01	–	0.01	0.02	0.01	0.01	0.09	0.07	0.05	0.06	0.08	0.07
P^{Ethyne}_{CHOCHO}	0.01	0.01	0.01	0.01	0.01	0.01	0.04	0.04	0.03	0.03	0.03	0.03
$P^{Aromatics}_{CHOCHO}$	0.60	0.26	0.15	0.22	0.21	0.09	0.26	0.19	0.09	0.28	0.20	0.11
$P^{Isoprene}_{CHOCHO}$	0.07	0.09	0.12	0.13	0.29	0.35	0.44	0.43	0.31	0.83	0.90	1.06
P^{Total}_{CHOCHO}	0.69	0.35	0.28	0.39	0.52	0.46	0.86	0.74	0.49	1.21	1.24	1.27
	NMHC reactivities, s^{-1}											
Alkanes	4.87	2.63	2.3	3.46	1.67	0.85	0.17	0.14	0.15	0.62	0.17	0.18
Alkenes	4.47	3.46	3.43	3.0	3.16	5.18	1.22	0.89	0.87	1.44	1.2	1.6
Ethyene	0.03	0.03	0.03	0.03	0.03	0.03	0.03	0.03	0.03	0.03	0.03	0.03
Aromatics	4.99	6.01	5.09	3.33	3.11	3.34	0.13	0.13	0.12	0.9	0.21	0.26
Isoprene	0.8	2.97	2.94	2.07	2.88	7.5	2.21	2.3	2.22	3.9	7.26	7.13
Total	15.16	15.1	13.79	11.89	10.85	16.9	3.76	3.49	3.39	6.88	8.88	9.2
	Radical and trace gas concentrations											
OH, 10^6 cm^{-3}	2.32	1.58	1.36	2.54	2.23	1.51	13.4	11.71	9.06	8.09	9.95	9.68
O_3, ppb	13.65	15.25	18.65	23.8	31.97	17.26	74.07	67.1	61.61	32.64	68.45	56.91
NO, ppb	4.36	6.81	7.43	0.38	1.44	1.71	0.1	0.11	0.09	0.39	0.08	0.17
NO_2, ppb	18.99	20.34	21.6	13.04	18.03	20.01	1.59	1.18	1.34	5.81	2.01	2.14

ACPD
13, 33013–33054, 2013

Table 4. Relative changes of HCHO and CHOCHO mixing ratio and R_{GF} under different model simulations (Table 1) for the PRIDE-PRD2006 campaign. When the model scenario is changing from M_i to M_j ($i, j \in [0,4]$), the relative change in percentage is calculated as $\% = 100 \times (M_j - M_i)/M_i$.

Model	Time Period (in LT)	Relative change in %		
		HCHO	CHOCHO	R_{GF}
M0 → M1	06:00–18:00	−49	−37	22
	06:00–10:00	−41	−22	31
	10:00–18:00	−53	−44	18
M1 → M2	06:00–18:00	−16	−7	13
	06:00–10:00	−34	−16	30
	10:00–18:00	−7	−3	4
M2 → M3	06:00–18:00	−25	−30	−8
	06:00–10:00	−36	−40	−7
	10:00–18:00	−19	−26	−9
M3 → M4	06:00–18:00	−49	−45	4
	06:00–10:00	−66	−71	−14
	10:00–18:00	−40	−32	13
M0 → M4	06:00–18:00	−84	−79	30
	06:00–10:00	−92	−89	38
	10:00–18:00	−80	−74	26

ACPD
13, 33013–33054, 2013

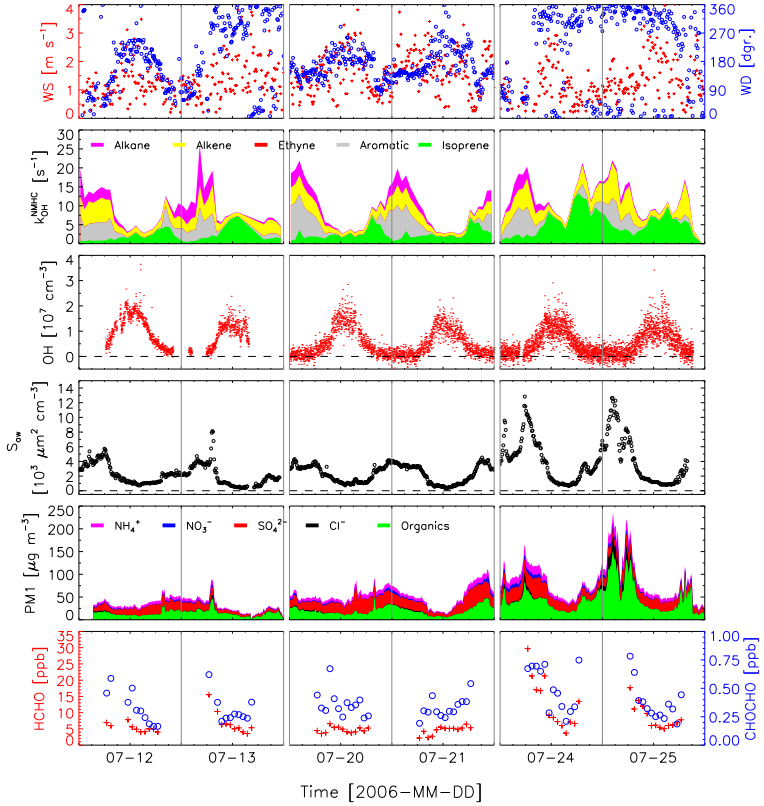

Fig. 1. Time series of wind speed (WS), wind direction (WD), OH reactivity of measured C3–C12 NMHCs (k_{OH}^{NMHC}), OH, aerosol (PM_1) compositions, aerosol (PM_{10}) surface concentration (S_{aw}, i.e., S_a corrected for hygroscopic growth), HCHO, and CHOCHO for the 6 cloud-free days during the PRIDE-PRD2006 campaign. S_{aw} is the RH corrected aerosol surface concentration, i.e., $S_{aw} = S_a \times f(RH) = S_a \times (1 + a \times (RH)^b)$. The empirical factors a and b used to estimate $f(RH)$ were set to 2.06 and 3.6 as described by Liu et al. (2008).

ACPD
13, 33013–33054, 2013

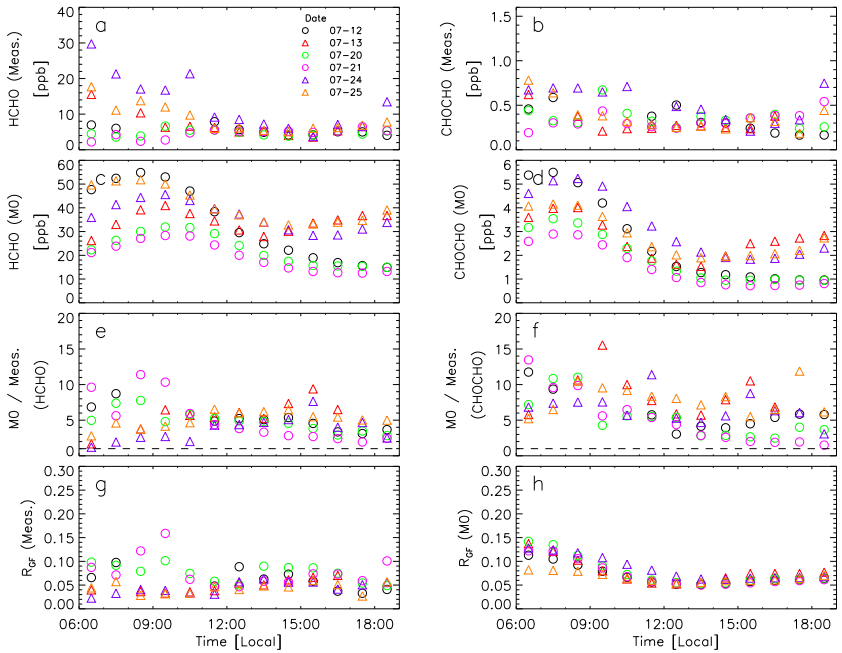

Fig. 2. Measured and modeled HCHO, CHOCHO, and CHOCHO/HCHO ratios (R_{GF}) for the 6 cloud-free days during the PRIDE-PRD2006 campaign. The modeled values are from the model base-case (M0). M0/Meas. represents the ratio between the modeled and measured concentration. Data of G1 and G2 days as described in the text are displayed as open circles and triangles, respectively.

ACPD
13, 33013–33054, 2013

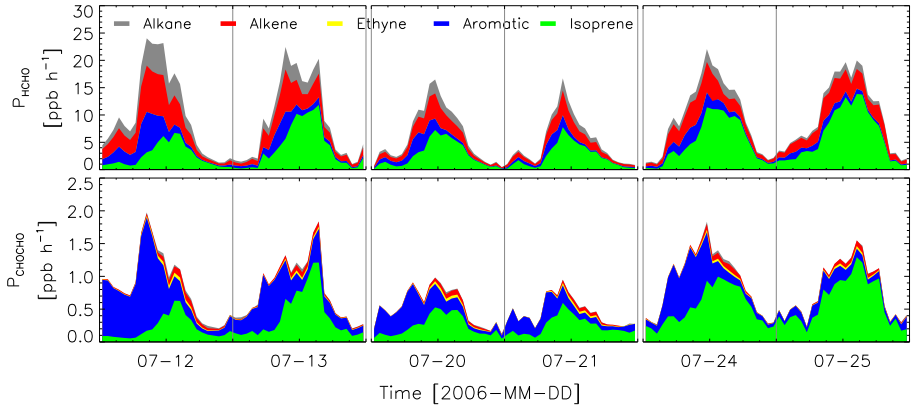

Fig. 3. Production of HCHO and CHOCHO from different NMHCs precursors in the model base-case (M0) for the 6 cloud-free days during the PRIDE-PRD2006 campaign.

ACPD
13, 33013–33054, 2013

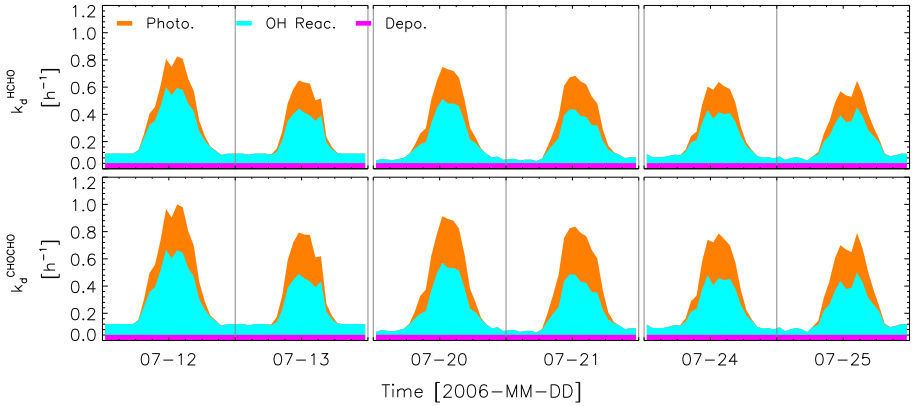

Fig. 4. Destruction of HCHO and CHOCHO, expressed as the sum of first order reaction rate of reaction with OH, photolysis, and deposition, in the model base-case (M0) for the 6 cloud-free days during the PRIDE-PRD2006 campaign.

ACPD
13, 33013–33054, 2013

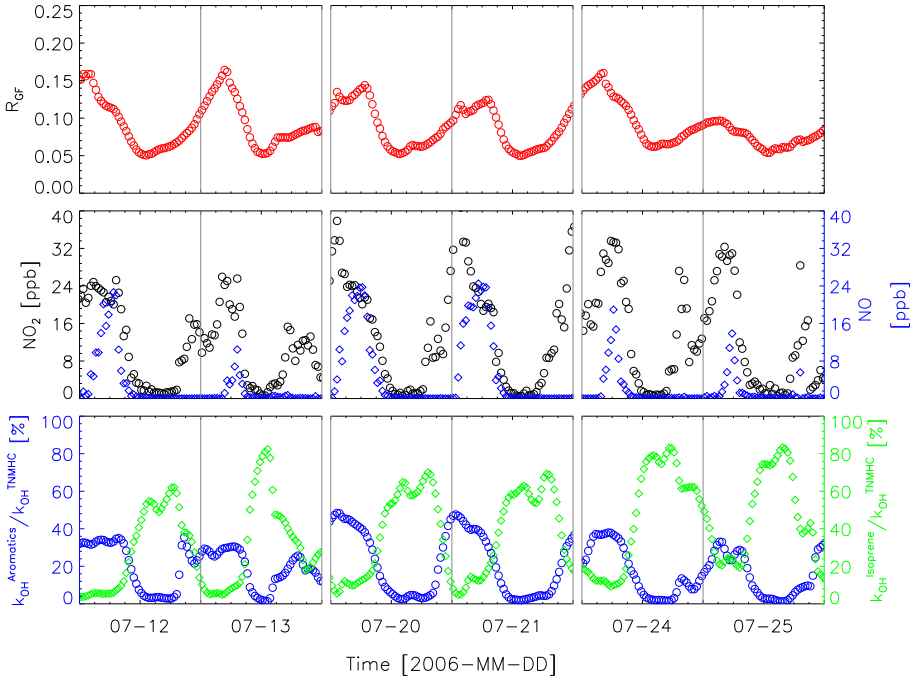

Fig. 5. Time series of modeled (model M0) R_{GF}, measured NO and NO_2 concentrations and NMHC compositions for the 6 cloud-free days during the PRIDE-PRD2006 campaign. The NMHC composition is expressed as the fraction of OH reactivity of a certain type of NMHC to that of the total NMHC.

ACPD
13, 33013–33054, 2013

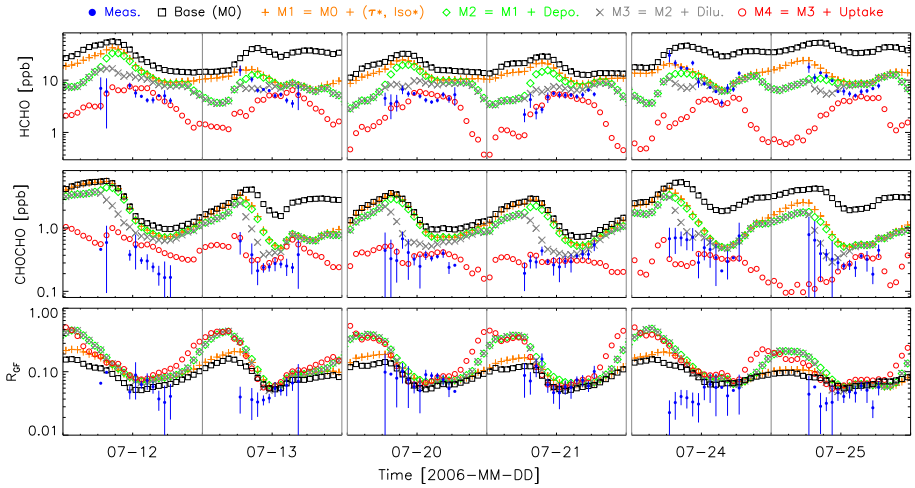

Fig. 6. Sensitivity analysis of HCHO and CHOCHO simulation for the 6 cloud-free days during the PRIDE-PRD2006 campaign. The blue dots are the measured concentrations with error bars indicating the 1σ error of the measurements. Symbols with color black, orange, green, gray, and red represent the modeled concentrations by model base-case M0, and M1–M4, respectively. Detailed model settings are described in Table 1 in the text.

ACPD
13, 33013–33054, 2013